

\mathbb{Z}_2 topological quantum paramagnet on a honeycomb bilayer

Darshan G. Joshi* and Andreas P. Schnyder†

Max-Planck-Institute for Solid State Research, D-70569 Stuttgart, Germany



(Received 27 September 2018; published 26 July 2019)

Topological quantum paramagnets are exotic states of matter, whose magnetic excitations have a topological band structure, while the ground state is topologically trivial. Here we show that a simple model of quantum spins on a honeycomb bilayer hosts a time-reversal-symmetry protected \mathbb{Z}_2 topological quantum paramagnet (*topological triplon insulator*) in the presence of spin-orbit coupling. The excitation spectrum of this quantum paramagnet consists of three triplon bands, two of which carry a nontrivial \mathbb{Z}_2 index. As a consequence, there appear two counterpropagating triplon excitation modes at the edge of the system. We compute the triplon edge state spectrum and the \mathbb{Z}_2 index for various parameter choices. We further show that upon making one of the Heisenberg couplings stronger, the system undergoes a topological quantum phase transition, where the \mathbb{Z}_2 index vanishes, to a different topological quantum paramagnet. In this case the counterpropagating triplon edge modes are disconnected from the bulk excitations and are protected by a chiral and a unitary symmetry. We discuss possible realizations of our model in real materials, in particular d^4 Mott insulators, and their potential applications.

DOI: [10.1103/PhysRevB.100.020407](https://doi.org/10.1103/PhysRevB.100.020407)

Introduction. The topology of quasiparticle band structures is of great interest for fundamental science and possible technological applications [1–4]. Not only fermionic but also bosonic quasiparticles can exhibit topological band structures. This has been demonstrated in a number of artificial systems, such as for electromagnetic waves in dielectric superlattices [5,6] or for polaritons in microcavities [7]. Bosonic quasiparticles with topological properties can also arise intrinsically in a variety of materials, e.g., as topological phonons in systems with isostatic lattices [8] as topological spin excitations in quantum magnets [9–20], or as topological triplon bands in dimerized magnets [21], which have been observed experimentally [22].

The study of topological spin excitations is enjoying growing activity, both due to its fundamental importance and its potential relevance for magnonic devices [23]. For example, topological magnon [11–17] and triplon insulators [21,22], as well as Dirac [19,20] and Weyl magnon semimetals [18] have been investigated. The magnon and triplon bands in these quantum magnets carry a nonzero Chern number, which by the bulk-boundary correspondence, gives rise to chiral magnon and triplon modes at the surface. Since these chiral surface modes carry spin with low dissipation and are protected against disorder, they could be utilized as efficient channels for spin transport [24]. However, in contrast to electronic topological insulators, the chiral surface magnons and triplons are excited states with an energy considerably higher than the bulk Goldstone modes of the ordered magnet. Hence, due to coupling to the low-energy bulk modes, these topological surface magnons and triplons are strongly damped [25], which suppresses the surface spin transport.

Recently, it was shown that topological spin excitations can also exist in the quantum-disordered paramagnetic phase of a spin ladder [10]. This one-dimensional topological quantum paramagnet exhibits protected triplon end states. For applications it would be advantageous to have a *two-dimensional* version of this quantum paramagnet, with protected triplon edge states forming a robust channel for spin transport [26].

In this Rapid Communication, we provide an example of such a two-dimensional topological quantum paramagnet. We consider a spin-1/2 system of two coupled honeycomb layers, with strong antiferromagnetic exchange interactions between the layers and weaker intralayer Heisenberg and Dzyaloshinskii-Moriya (DM) interactions. The dominant interlayer antiferromagnetic exchange leads to a coupled-dimer ground state, where two spins form an interlayer spin singlet. The elementary excitations above this dimerized ground state are gapped triplons, corresponding to the breaking of singlet dimers into spin-1 triplet states. We find that these triplons, which are bosonic quasiparticles with $S = 1$, exhibit a nontrivial topological band structure, which is characterized by a \mathbb{Z}_2 index, akin to the quantum spin Hall effect [27]. As a result, the triplons exhibit exotic behaviors, such as a triplon spin Hall effect and counterpropagating triplon edge modes. We note that these triplons are different from Refs. [21,22], where the triplon bands have a Chern index, break time-reversal symmetry and occur in an ordered phase.

Model description. Our model consists of $S = 1/2$ spins on a bilayer honeycomb lattice (Fig. 1) with the following Hamiltonian:

$$\mathcal{H} = \sum_i J_i \vec{S}_{1i} \cdot \vec{S}_{2i} + \sum_{\langle ij \rangle} K_{ij} [\vec{S}_{1i} \cdot \vec{S}_{1j} + \vec{S}_{2i} \cdot \vec{S}_{2j}] + \sum_{\langle\langle ij \rangle\rangle} D_{ij} [S_{1i}^x S_{1j}^y - S_{1j}^x S_{1i}^y + S_{2i}^x S_{2j}^y - S_{2j}^x S_{2i}^y], \quad (1)$$

*d.joshi@fkf.mpg.de

†a.schnyder@fkf.mpg.de

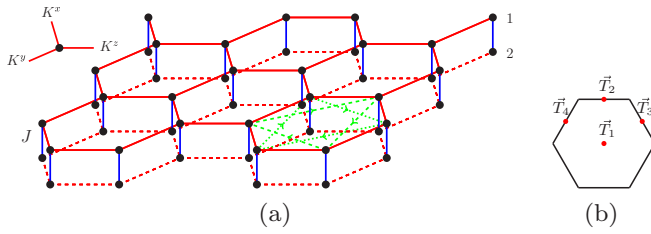


FIG. 1. (a) Honeycomb bilayer model with $S = 1/2$ spins indicated by the black dots. Blue lines represent the interlayer antiferromagnetic interactions, while red solid/dashed lines correspond to the anisotropic intralayer exchange. The DM interaction is perpendicular to the honeycomb layers. Along the green lines, in the direction of an arrow $D_{ij} = D$ and $D_{ji} = -D_{ij}$ (shown only on one hexagonal plaquette). (b) Hexagonal first Brillouin zone with the red dots indicating the time-reversal invariant momenta.

where i labels the dimer lattice sites and the indices 1,2 denote the two honeycomb layers. The first term in Eq. (1) is the antiferromagnetic ($J_i > 0$) interlayer Heisenberg interaction, where we allow for a staggered on-site potential such that $J_i = J \pm \alpha$ ($\alpha \ll J$) on sublattice A (B). The second term in Eq. (1) represents the nearest-neighbor Heisenberg interaction within a layer, and the last term is the next-nearest-neighbor DM interaction. Note that we have allowed for anisotropic Heisenberg interactions within a layer [see Fig. 1(a)] such that $K_{ij} = K^\alpha$ along the α bond ($\alpha = x, y, z$). For simplicity, we shall consider $K^x = K^y \equiv K$ such that the interaction K^z introduces anisotropy, which could be realized in real materials by applying uniaxial pressure. We note that the DM interaction is perpendicular to the honeycomb layers such that $D_{ij} = D(-D)$ when going clockwise (anticlockwise) in a hexagonal plaquette [see Fig. 1(a)].

We are interested in the dimer-paramagnetic phase, described by a product state of singlets, which is realized for dominant $J > 0$. In this phase there are three gapped quasiparticle excitation bands, corresponding to the three spin-1 triplet excited states on each dimer $|t_x\rangle = -[|\uparrow\uparrow\rangle - |\downarrow\downarrow\rangle]/\sqrt{2}$, $|t_y\rangle = \iota[|\uparrow\uparrow\rangle + |\downarrow\downarrow\rangle]/\sqrt{2}$, and $|t_z\rangle = [|\uparrow\downarrow\rangle + |\downarrow\uparrow\rangle]/\sqrt{2}$, over the singlet state $|t_0\rangle = [|\uparrow\downarrow\rangle - |\downarrow\uparrow\rangle]/\sqrt{2}$. To describe the band structure of these triplon excitations we employ the bond-operator formalism [28], wherein the triplon quasiparticles are expressed in terms of the triplon creation and annihilation operators t_γ^\dagger and t_γ ($\gamma = x, y, z$), defined as $t_\gamma^\dagger|t_0\rangle = |t_\gamma\rangle$. Inserting the triplon representation of the spin operators into Eq. (1) yields an interacting triplon Hamiltonian [29]. For simplicity, we shall work within the harmonic approximation, retaining only the bilinear part of the triplon Hamiltonian. This approximation is justified, since deep inside the paramagnetic phase the triplon density is small, which allows one to neglect any triplon interactions [30]. Within the harmonic approximation, the t_z mode is decoupled from the t_x and t_y modes. For that reason, we focus on the t_x and t_y excitations, whose dynamics in momentum space is described by $\mathcal{H}_2 = \frac{1}{2} \sum_{\vec{k}} \Psi_{\vec{k}}^\dagger \mathcal{M}_{\vec{k}} \Psi_{\vec{k}}$, with the 8×8 matrix

$$\mathcal{M}_{\vec{k}} = \begin{pmatrix} h_{1,\vec{k}} & h_{2,\vec{k}} \\ h_{2,\vec{k}}^\dagger & h_{1,-\vec{k}}^T \end{pmatrix} \quad (2)$$

and $\Psi_{\vec{k}} = (t_{\vec{k}x}^A, t_{\vec{k}y}^A, t_{\vec{k}x}^B, t_{\vec{k}y}^B, t_{-\vec{k}x}^{A\dagger}, t_{-\vec{k}y}^{A\dagger}, t_{-\vec{k}x}^{B\dagger}, t_{-\vec{k}y}^{B\dagger})^T$, where the superscripts A/B label the two honeycomb sublattices. For now we set the staggered on-site potential $\alpha = 0$. The matrix elements of $\mathcal{M}_{\vec{k}}$, $h_{2,\vec{k}} = h_{1,\vec{k}} - J\mathbb{1} = \vec{d} \cdot \vec{\Gamma}$, are given in terms of the \vec{d} vector,

$$\vec{d} = \{\text{Re}(\kappa_{\vec{k}}), -\text{Im}(\kappa_{\vec{k}}), 0, -2D\gamma'_{\vec{k}}, 0\}, \quad (3)$$

and the five Dirac matrices $\vec{\Gamma} = \{\sigma_1 \otimes \mathbb{1}, \sigma_2 \otimes \mathbb{1}, \sigma_3 \otimes \tau_1, \sigma_3 \otimes \tau_2, \sigma_3 \otimes \tau_3\}$. Here σ_i and τ_i are the Pauli matrices acting on the sublattice and the triplon-flavor spaces, respectively. The parameters $\kappa_{\vec{k}}$ and $\gamma'_{\vec{k}}$ in Eq. (3) are defined as follows:

$$\kappa_{\vec{k}} = \frac{1}{2}[K^z + Ke^{i\vec{k}_1} + Ke^{i\vec{k}_2}], \quad (4)$$

$$\gamma'_{\vec{k}} = -\sin(\vec{k}_1) + \sin(\vec{k}_2) + \sin(\vec{k}_1 - \vec{k}_2), \quad (5)$$

where $\vec{k}_{1,2} = \vec{k} \cdot \vec{a}_{1,2}$, with $\vec{a}_{1,2} = \{\pm\hat{x}/2, \sqrt{3}\hat{y}/2\}$ being the Bravais basis vectors.

Triplon dynamics and edge states. To compute the triplon dispersions, we have to evaluate the eigenvalues of the non-Hermitian matrix $\Sigma \mathcal{M}_{\vec{k}}$, where $\Sigma = \sigma_3 \otimes \mathbb{1}_{4 \times 4}$ [31]. Since $[h_{1,\vec{k}}, h_{2,\vec{k}}] = 0$, the eigenvalues of $\Sigma \mathcal{M}_{\vec{k}}$ are obtained in a straightforward manner. For the t_x and t_y triplons the dispersion is

$$\omega_{A,B}^{x/y} = \sqrt{J(J \pm 2\sqrt{4D^2\gamma_{\vec{k}}'^2 + |\kappa_{\vec{k}}|^2})}, \quad (6)$$

while for the t_z triplon it reads $\omega^z = \sqrt{J(J \pm 2|\kappa_{\vec{k}}|)}$. We now exclusively focus on the t_x and t_y bands, since the t_z band is topologically trivial. It is clear from Eq. (6) that in the absence of the DM interaction and as long as $|K^z| < 2K$, the triplon bands cross each other at two points in the Brillouin zone (BZ). Since these two band crossings are fourfold degenerate and the dispersion is linear in their vicinity, they realize triplon analogs of Dirac fermions, i.e., ‘‘Dirac triplons.’’ The topological character of these Dirac triplons manifests itself in the edge spectrum in terms of dispersionless triplon edge states, which connect the two Dirac points [see Fig. S1 in the Supplemental Material (SM) [29]].

Upon introducing the DM interaction, a topological gap is opened at the two Dirac points. Two counterpropagating triplon edge states appear within this gap, which connect the t_x and t_y bulk bands to each other (see Fig. 2). These are protected by the time-reversal symmetry. We may call this state a ‘‘topological triplon insulator,’’ since its edge-state spectrum is identical to that of the two-dimensional electronic topological insulator [1]. However, as opposed to electronic topological insulators, the edge states of the topological triplon insulator are excited states, which cross at an energy of the order J above the ground-state energy. Hence, in order to probe the physics of these triplon edge states, they need to be thermally populated or excited out of equilibrium.

In Fig. 2 we show how the triplon edge states evolve as a function of the anisotropy in the intralayer Heisenberg interaction K^z/K . Upon increasing K^z relative to K , the gapped Dirac triplons move along the edges of the bulk BZ until they merge at the M point for $K^z = 2K$, where they form a quadratic band touching [Fig. 2(c)]. In this process, the

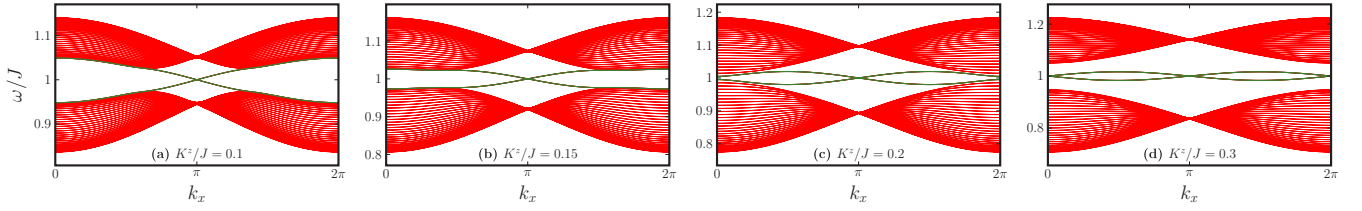


FIG. 2. Triplon bands in the presence of the DM interaction with open boundaries along the zigzag edge. The edge states, which are located around $J = 1$, are indicated in green. For $|K^z| < 2K$, a \mathbb{Z}_2 topological quantum paramagnet is realized, which has similar band structure and edge state as the quantum spin Hall effect. At $|K^z| = 2K$ a topological phase transition occurs, which separates the \mathbb{Z}_2 topological phase from a quantum paramagnet with edge states that are detached from the bulk bands. The parameters used in these plots are $K/J = 0.1$, $D/J = 0.01$, and $\alpha/J = 0$.

crossing of the triplon edge states gets stretched out, until at $K^z = 2K$ the edge states touch at both $k_x = 0$ and $k_x = \pi$. Further increasing K^z/K , a bulk gap opens up again and the edge states detach from the bulk bands. In fact, for $K^z > 2K$ the triplon edge states lie completely in the bulk gap, without touching the bulk triplon bands at all [Fig. 2(d)]. We will see below that the bulk gap closing at $K^z = 2K$ corresponds to a topological phase transition, which separates two distinct topological phases with two different types of edge states: For $K^z < 2K$ there are two edge states attached to the bulk bands and protected by a \mathbb{Z}_2 invariant, while for $K^z > 2K$ the edge states are detached from the bulk bands and protected by chiral symmetry. In the Supplemental Material [29] we also discuss the effect of staggered potential α . The full phase diagram as a function of both α and K^z is shown in Fig. 3. In passing, we remark that these types of detached edge states can be realized, in principle, also in fermionic systems [29].

\mathbb{Z}_2 topological invariant. In order to establish the topological origin of the edge states discussed above, we show that they are protected by a \mathbb{Z}_2 invariant, which can be defined in the presence of the time-reversal symmetry. In the presence of parity symmetry (i.e., when $\alpha = 0$), the \mathbb{Z}_2 invariant ν can

be expressed in terms of the parity eigenvalues of the triplon bands [27], i.e.,

$$(-1)^\nu = \prod_{i=1}^4 \delta_i, \tag{7}$$

where $\delta_i = \delta(\vec{T}_i)$ gives the parity eigenvalue of the lower triplon band at the four time-reversal invariant momenta \vec{T}_i [see Fig. 1(c)]. Parity symmetry acts on the triplon Hamiltonian (2) as $\hat{P}\mathcal{M}_{\vec{k}}\hat{P}^{-1} = \mathcal{M}_{-\vec{k}}$, with the parity operator $\hat{P} = \mathbb{1} \otimes \Gamma_1$.

Note that for our bosonic problem the relevant matrix is not $\mathcal{M}_{\vec{k}}$, but rather $\Sigma\mathcal{M}_{\vec{k}}$, which, however, obeys the same parity symmetry as $\mathcal{M}_{\vec{k}}$, since $[\hat{P}, \Sigma] = 0$. Recall that for the honeycomb lattice, there are four time-reversal invariant momenta: $\vec{T}_1 = \{0, 0\}$, $\vec{T}_2 = \{0, 2\pi/\sqrt{3}\}$, $\vec{T}_3 = \{\pi, \pi/\sqrt{3}\}$, and $\vec{T}_4 = \{-\pi, \pi/\sqrt{3}\}$ [see Fig. 1(b)]. At these time-reversal invariant momenta, $[\hat{P}, \mathcal{M}_{\vec{T}_i}] = 0$ as well as $[\hat{P}, \Sigma\mathcal{M}_{\vec{T}_i}] = 0$. It is now straightforward to see that the parity eigenvalue of the lower triplon band is related to the sign of $d_1 = \text{Re}(\kappa_{\vec{k}})$. Hence, from Eq. (4) we find that

$$\delta_i = -\text{sgn} \left\{ \frac{1}{2} \left[K^z + 2K \cos\left(\frac{k_x}{2}\right) \cos\left(\frac{\sqrt{3}k_y}{2}\right) \right] \right\}.$$

At the four time-reversal invariant momenta we have

$$d_1(\vec{T}_{1,2}) = \frac{K^z \pm 2K}{2}; \quad d_1(\vec{T}_{3,4}) = \frac{K^z}{2}. \tag{8}$$

It follows that for $K > 0$ the \mathbb{Z}_2 invariant is given by

$$\nu = \begin{cases} 0, & \text{if } |K^z| > 2K \\ 1, & \text{if } |K^z| < 2K. \end{cases} \tag{9}$$

Thus, for $|K^z| < 2K$ the triplon spectrum is topological, in agreement with the appearance of edge states, as discussed above. Due to its topological excitation spectrum, we call the phase $|K^z| < 2K$ a *\mathbb{Z}_2 topological quantum paramagnet*.

In the absence of parity symmetry (i.e., when $\alpha \neq 0$), formula (7) for the \mathbb{Z}_2 topological invariant ν is no longer valid. However, in this case we can consider an adiabatic deformation, which smoothly transforms the Hamiltonian to a parity symmetric one, without closing the gap in the triplon spectrum. Alternatively, the \mathbb{Z}_2 invariant can be formulated in terms of the triplon eigenstates [32,33], which does not rely on the existence of a parity symmetry, but only the time-reversal symmetry.

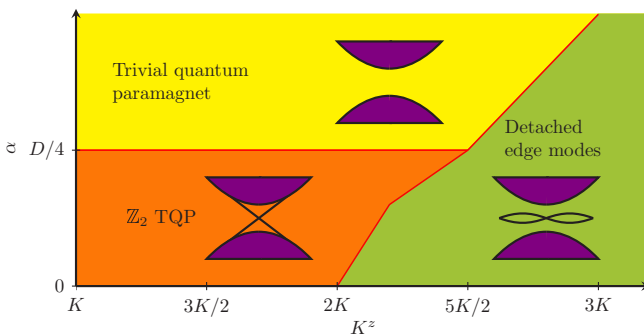


FIG. 3. Topological phase diagram as a function of the anisotropic Heisenberg interaction K^z and staggered on-site potential α in the presence of a finite DM interaction D . The lower left phase (orange) is the \mathbb{Z}_2 topological quantum paramagnet or the topological triplon insulator, which has counterpropagating edge modes connecting the bulk triplon modes. The right-side phase (green) is a topological quantum paramagnet with detached edge modes protected by chiral symmetry and realized for strongly anisotropic K^z . The upper phase (yellow) is a trivial quantum paramagnet with no edge excitations. The parameters used here are $K/J = 0.1$ and $D/J = 0.01$.

Another point to note is that the \mathbb{Z}_2 invariant is independent of the DM interaction. The role of the DM interaction is to just separate the triplon bulk bands. In fact, just as in the case of the quantum spin Hall effect, the absence of a DM interaction simply means that the triplon bands must touch at energy J for $|K^z| < 2K$ [27].

Protection of detached edge modes. The \mathbb{Z}_2 invariant (7) is zero for $|K^z| > 2K$. Nevertheless, in this regime there appear edge states too, which are protected by symmetry, as we will now show. To establish this, we first observe that besides the antiunitary time-reversal symmetry, the triplon Hamiltonian $\mathcal{M}_{\vec{k}}$, Eq. (2), also exhibits a unitary symmetry, i.e., it commutes with $\hat{G} = \mathbb{1}_{4 \times 4} \otimes \tau_2$. Moreover, the model possesses a type of chiral symmetry, that is, $\mathcal{M}_{\vec{k}} - J\mathbb{1}$ anticommutes with the chiral operator $\hat{C} = \mathbb{1} \otimes \sigma_3 \otimes \tau_3$. Since both of these symmetries also hold for $\Sigma\mathcal{M}_{\vec{k}}$, it follows that (i) the triplon bands can be labeled by the eigenvalues of \hat{G} and (ii) the triplon bands are symmetric around the energy J .

We can investigate the edge-state wave function near $k_x = 0$ by making an ansatz: $\Psi_{ed}(y) = e^{-\lambda y}\Phi$. It turns out that $\lambda = (K^z - 2K)/\sqrt{3}K$, which means that these edge modes exist only when $K^z > 2K$ (green region in Fig. 3). We refer to the Supplemental Material [29] for technical details. We quote here the full wave function of the detached edge states, $\Phi_{1,2} = (u\phi_{1,2}, v\phi_{1,2})^T$, where $u^2 - v^2 = 1$, which follows from the bosonic Bogoliubov transformation and $\phi_{1,2} = (\varphi_{\pm}, 0)^T$, with φ_{\pm} the eigenfunctions of τ_2 (i.e., $\tau_2\varphi_{\pm} = \pm\varphi_{\pm}$).

From above we infer that the two edge states $\Phi_{1,2}$ have opposite eigenvalues with respect to \hat{G} , i.e., $\hat{G}\Phi_{1,2} = \pm\Phi_{1,2}$. Hence, since \hat{G} commutes with $\Sigma\mathcal{M}_{\vec{k}}$, any hybridization between the two edge modes is prohibited by the symmetry \hat{G} . Moreover, we find that chiral symmetry \hat{C} converts one edge state into another (i.e., $\hat{C}\Phi_{1,2} = -\Phi_{2,1}$) and that parity \hat{P} guarantees the degeneracy between states on opposite edges. Therefore, away from $k_x = 0$ there is always exactly one edge state with $\epsilon < J$ and one edge state with $\epsilon > J$, and hence the $k_x = 0$ band crossing is pinned at $\epsilon = J$ [34]. Furthermore, we observe that as we let $k_x \rightarrow -k_x$ the \hat{G} eigenvalues of the $\epsilon_{1,2}$ eigenstates get interchanged. For this reason and due to the 2π periodicity of the wave functions, there must be another crossing of the edge states between 0 and π . Due to time-reversal symmetry this second crossing is pinned at $k_x = \pi$.

Conclusions and implications for experiments. The topological triplon edge modes could potentially be used as robust and efficient channels for spin transport. Their topological origin protects them against disorder scattering. The triplon

edge modes should be observable in various experimental probes [35]. For example, neutron-scattering experiments should be able to detect a pronounced peak in the dynamical spin structure factor at the energy of the triplon edge states (see SM [29] for a detailed prediction). Another possibility is to measure spin Hall noise in a normal metal deposited on top of the honeycomb bilayer paramagnet, which is expected to show signatures of the triplon edge states [36]. Apart from this, thermal or spin transport measurements could also probe these nontrivial edge modes [24]. However, unlike fermionic topological states there is no quantized response, which makes it challenging to find an unambiguous physical observable of the nontrivial topology.

The topological triplon edge states discussed in this Rapid Communication are expected to occur in a wide range of model systems and materials. A promising set of materials is that of chromium trihalides, CrX_3 ($X = \text{F, Cl, Br, I}$), which are layered honeycomb materials with relevant interlayer coupling. These were of great interest in the past as a prototypical example of Heisenberg ferromagnets [37,38], but have since then been forgotten. However, recently they have been shown to host Dirac magnons [39]. It might be possible to realize a singlet ground state in these systems with the application of external pressure or by substituting chromium with some other transition metal. Moreover, the physics discussed in this work is expected to exist also in other bilayer systems with strong spin-orbit coupling, such as triangular- or square-lattice bilayer structures with dimerized ground states [29]. This might be of relevance (after appropriate substitution) for $\text{BaCuSi}_2\text{O}_6$ [40], which exhibits a spin-singlet dimerized ground state in a square-lattice bilayer structure.

Topological triplons can also arise in various spin-orbital systems realizing the singlet-triplet phenomenon. In particular, d^4 Mott insulators such as Li_2RuO_3 [41] and $\text{Ag}_3\text{LiRu}_2\text{O}_6$ [42], where transition metal ions form a honeycomb lattice, are promising candidates as they display singlet-triplet physics due to strong spin-orbit coupling [43,44]. It will be interesting to work out the conditions under which the triplon edge states can arise in these d^4 Mott insulators. It may be extended to d^8 Mott insulators as well [45]. Another direction for future research is the study of magnetic quantum phase transitions from a topological quantum paramagnet to a magnetically ordered phase. There are indications that the ordered phase might also host topological edge excitations [46]. However, this might require exact numerical studies.

Acknowledgment. We thank G. Khaliullin and H. Takagi for useful discussions.

[1] M. Z. Hasan and C. L. Kane, *Rev. Mod. Phys.* **82**, 3045 (2010).
 [2] C.-K. Chiu, J. C. Y. Teo, A. P. Schnyder, and S. Ryu, *Rev. Mod. Phys.* **88**, 035005 (2016).
 [3] A. Bansil, H. Lin, and T. Das, *Rev. Mod. Phys.* **88**, 021004 (2016).
 [4] N. P. Armitage, E. J. Mele, and A. Vishwanath, *Rev. Mod. Phys.* **90**, 015001 (2018).
 [5] Z. Wang, Y. Chong, J. D. Joannopoulos, and M. Soljacic, *Nature (London)* **461**, 772 (2009).

[6] L. Lu, Z. Wang, D. Ye, L. Ran, L. Fu, J. D. Joannopoulos, and M. Soljačić, *Science* **349**, 622 (2015).
 [7] P. St-Jean, V. Goblot, E. Galopin, A. Lemaître, T. Ozawa, L. Le Gratiet, I. Sagnes, J. Bloch, and A. Amo, *Nat. Photonics* **11**, 651 (2017).
 [8] C. L. Kane and T. C. Lubensky, *Nat. Phys.* **10**, 39 (2013).
 [9] S. A. Owerre, *Sci. Rep.* **7**, 6931 (2017).
 [10] D. G. Joshi and A. P. Schnyder, *Phys. Rev. B* **96**, 220405(R) (2017).

- [11] S. K. Kim, H. Ochoa, R. Zarzuela, and Y. Tserkovnyak, *Phys. Rev. Lett.* **117**, 227201 (2016).
- [12] S. A. Owerre, *Phys. Rev. B* **94**, 094405 (2016).
- [13] S. A. Owerre, *J. Phys.: Condens. Matter* **28**, 386001 (2016).
- [14] S. A. Owerre, *J. Appl. Phys.* **120**, 043903 (2016).
- [15] B. Xu, T. Ohtsuki, and R. Shindou, *Phys. Rev. B* **94**, 220403(R) (2016).
- [16] D. G. Joshi, *Phys. Rev. B* **98**, 060405(R) (2018).
- [17] P. A. McClarty, X.-Y. Dong, M. Gohlke, J. G. Rau, F. Pollmann, R. Moessner, and K. Penc, *Phys. Rev. B* **98**, 060404(R) (2018).
- [18] F.-Y. Li, Y.-D. Li, Y. B. Kim, L. Balents, Y. Yu, and G. Chen, *Nat. Commun.* **7**, 12691 (2016).
- [19] K. Li, C. Li, J. Hu, Y. Li, and C. Fang, *Phys. Rev. Lett.* **119**, 247202 (2017).
- [20] W. Yao, C. Li, L. Wang, S. Xue, Y. Dan, K. Iida, K. Kamazawa, K. Li, C. Fang, and Y. Li, *Nat. Phys.* **14**, 1011 (2018).
- [21] J. Romhányi, K. Penc, and R. Ganesh, *Nat. Commun.* **6**, 6805 (2015).
- [22] P. A. McClarty, F. Krüger, T. Guidi, S. F. Parker, K. Refson, A. W. Parker, D. Prabhakaran, and R. Coldea, *Nat. Phys.* **13**, 736 (2017).
- [23] B. Lenk, H. Ulrichs, F. Garbs, and M. Münzenberg, *Phys. Rep.* **507**, 107 (2011).
- [24] A. Rückriegel, A. Brataas, and R. A. Duine, *Phys. Rev. B* **97**, 081106(R) (2018).
- [25] A. L. Chernyshev and P. A. Maksimov, *Phys. Rev. Lett.* **117**, 187203 (2016).
- [26] In contrast to the magnon [11–20] and triplon [21,22] surface states of the aforementioned ordered magnets, the triplon end states of the quantum-disordered paramagnet [10] are only weakly damped due to energy-momentum constraints and the absence of Goldstone modes.
- [27] L. Fu and C. L. Kane, *Phys. Rev. B* **76**, 045302 (2007).
- [28] S. Sachdev and R. N. Bhatt, *Phys. Rev. B* **41**, 9323 (1990).
- [29] See Supplemental Material at <http://link.aps.org/supplemental/10.1103/PhysRevB.100.020407>, which includes Ref. [47–51], for the derivation of the triplon Hamiltonian, the discussion of the spectrum in the absence of DM interaction, effect of staggered potential, details of detached edge modes protection, the computation of the dynamical structure factor, and the derivation of the square-lattice bilayer model.
- [30] In general, the harmonic approximation is controlled in large dimensions, both in the paramagnetic as well as inside the magnetically ordered phases, as shown in Refs. [52,53].
- [31] J.-P. Blaizot and G. Ripka, *Quantum Theory of Finite Systems* (MIT Press, Cambridge, 1986).
- [32] C. L. Kane and E. J. Mele, *Phys. Rev. Lett.* **95**, 146802 (2005).
- [33] L. Fu and C. L. Kane, *Phys. Rev. B* **74**, 195312 (2006).
- [34] In the absence of parity (i.e., for $\alpha \neq 0$), the edge states on opposite edges split in energy, but are still symmetric around J .
- [35] Triplon-triplon scattering is weak, because of the dilute density of triplons, provided we are away from a magnetic quantum critical point. Moreover, the interaction-induced damping of the triplon edge modes is suppressed, due to the absence of Goldstone modes and due to phase-space constraints, as long as the bulk triplon gap is larger than $J/2$.
- [36] D. G. Joshi, A. P. Schnyder, and S. Takei, *Phys. Rev. B* **98**, 064401 (2018).
- [37] E. J. Samuelsen, R. Silbergliitt, G. Shirane, and J. P. Remeika, *Phys. Rev. B* **3**, 157 (1971).
- [38] W. B. Yelon and R. Silbergliitt, *Phys. Rev. B* **4**, 2280 (1971).
- [39] S. S. Pershoguba, S. Banerjee, J. C. Lashley, J. Park, H. Ågren, G. Aeppli, and A. V. Balatsky, *Phys. Rev. X* **8**, 011010 (2018).
- [40] Y. Sasago, K. Uchinokura, A. Zheludev, and G. Shirane, *Phys. Rev. B* **55**, 8357 (1997).
- [41] Y. Miura, Y. Yasui, M. Sato, N. Igawa, and K. Kakurai, *J. Phys. Soc. Jpn.* **76**, 033705 (2007).
- [42] S. A. J. Kimber, C. D. Ling, D. J. P. Morris, A. Chemseddine, P. F. Henry, and D. N. Argyriou, *J. Mater. Chem.* **20**, 8021 (2010).
- [43] G. Khaliullin, *Phys. Rev. Lett.* **111**, 197201 (2013).
- [44] O. N. Meetei, W. S. Cole, M. Randeria, and N. Trivedi, *Phys. Rev. B* **91**, 054412 (2015).
- [45] F.-Y. Li and G. Chen, *Phys. Rev. B* **100**, 045103 (2019).
- [46] H. Kondo, Y. Akagi, and H. Katsura, *Phys. Rev. B* **99**, 041110 (2019).
- [47] A. Collins, C. J. Hamer, and Z. Weihong, *Phys. Rev. B* **74**, 144414 (2006).
- [48] C. L. Kane and E. J. Mele, *Phys. Rev. Lett.* **95**, 226801 (2005).
- [49] S. Wang, D. Scarabelli, L. Du, Y. Y. Kuznetsova, L. N. Pfeiffer, K. W. West, G. C. Gardner, M. J. Manfra, V. Pellegrini, S. J. Wind *et al.*, *Nat. Nanotech.* **13**, 29 (2018).
- [50] A. N. Rudenko and M. I. Katsnelson, *Phys. Rev. B* **89**, 201408(R) (2014).
- [51] M. Ezawa, *New J. Phys.* **16**, 115004 (2014).
- [52] D. G. Joshi, K. Coester, K. P. Schmidt, and M. Vojta, *Phys. Rev. B* **91**, 094404 (2015).
- [53] D. G. Joshi and M. Vojta, *Phys. Rev. B* **91**, 094405 (2015).